EXHIBIT 24

Assessing the Risk of Persistent Drought Using Climate Model Simulations and Paleoclimate Data

TOBY R. AULT

Department of Earth and Atmospheric Sciences, Cornell University, Ithaca, New York

JULIA E. COLE AND JONATHAN T. OVERPECK

Department of Geosciences and Department of Atmospheric Sciences, The University of Arizona, Tucson, Arizona

GREGORY T. PEDERSON

U.S. Geological Survey, Bozeman, Montana

DAVID M. MEKO

Laboratory of Tree-Ring Research, The University of Arizona, Tucson, Arizona

(Manuscript received 10 May 2012, in final form 4 November 2013)

ABSTRACT

Projected changes in global rainfall patterns will likely alter water supplies and ecosystems in semiarid regions during the coming century. Instrumental and paleoclimate data indicate that natural hydroclimate fluctuations tend to be more energetic at low (multidecadal to multicentury) than at high (interannual) frequencies. State-of-the-art global climate models do not capture this characteristic of hydroclimate variability, suggesting that the models underestimate the risk of future persistent droughts. Methods are developed here for assessing the risk of such events in the coming century using climate model projections as well as observational (paleoclimate) information. Where instrumental and paleoclimate data are reliable, these methods may provide a more complete view of prolonged drought risk. In the U.S. Southwest, for instance, state-of-the-art climate model projections suggest the risk of a decade-scale megadrought in the coming century is less than 50%; the analysis herein suggests that the risk is at least 80%, and may be higher than 90% in certain areas. The likelihood of longer-lived events (>35 yr) is between 20% and 50%, and the risk of an unprecedented 50-yr megadrought is nonnegligible under the most severe warming scenario (5%–10%). These findings are important to consider as adaptation and mitigation strategies are developed to cope with regional impacts of climate change, where population growth is high and multidecadal megadrought—worse than anything seen during the last 2000 years—would pose unprecedented challenges to water resources in the region.

1. Introduction

Information recorded in paleoclimate archives reveals that the twentieth century does not represent the full range of drought variability experienced in western North America (WNA) during the last millennium (e.g., Woodhouse and Overpeck 1998; Stahle et al. 2007; Cook et al. 2004; Meko et al. 2007). Prolonged droughts comprise a source of climate risk in this region and elsewhere (Woodhouse and Overpeck 1998; Shanahan et al. 2009; Buckley et al. 2010; Haug et al. 2003; deMenocal 2001). Decade-scale droughts like the 1930s Dust Bowl occur, on average, once or twice per century (Woodhouse and Overpeck 1998), and considerably longer periods of aridity (megadroughts) are also apparent in paleoclimate records (Woodhouse and Overpeck 1998). Were such megadroughts to occur today, they would exact regionally unprecedented socioeconomic tolls and

Denotes Open Access content.

Corresponding author address: Toby R. Ault, Dept. of Earth and Atmospheric Sciences, Bradfield Hall, Cornell University, Ithaca, NY 14853.
E-mail: toby.ault@cornell.edu

DOI: 10.1175/JCLI-D-12-00282.1

ecological consequences. For example, during the 1150s, the 25-yr average of reconstructed Colorado River flow dropped to 85% of the twentieth-century mean for 10 consecutive years (Meko et al. 2007). In modern terms, this would be comparable to losing almost the entire allocation for the state of Arizona from the long-term mean for a decade. What is perhaps even more problematic for water resource management is that the 1150s were centered in a 23-yr interval of below-average moisture across WNA, and a similar interval in the twelfth century spanned 22 yr (1276–99; Cook et al. 2007). Older tree-ring records suggest that regional droughts can persist, and have persisted, for longer still (~50 yr; Routson et al. 2011).

Prolonged droughts have happened during the instrumental era and include the 1930s Dust Bowl (Fye et al. 2003), drought in sub-Saharan Africa (e.g., Charney 1975; Folland et al. 1986), and the recent "Big Dry" in Australia (Leblanc et al. 2012). Since these events occur infrequently, it is difficult to understand their statistics using data from the instrumental era alone. Tree-ring reconstructions partially address this limitation, and in the U.S. Southwest they suggest that events similar to the 1150s Colorado River megadrought would be expected to occur every 400–600 yr (Meko et al. 2012). This view of risk is incomplete, however, because it is specific to the 1150s event and "megadrought risk" could be applied more generally to a wide range of time scales. More critically, the statistics of twenty-first-century climate will be influenced by anthropogenic greenhouse gases (GHG) (Solomon et al. 2007). The risk of future prolonged drought risk will therefore depend on the internal rate at which these events occur as well as any GHG-forced changes in their underlying statistics. In the U.S. Southwest, for instance, precipitation is projected to decrease as a consequence of GHG-forced changes (e.g., Seager et al. 2007; Solomon et al. 2007; Diffenbaugh and Giorgi 2012). Any assessment of future megadrought risk, therefore, should account for both the natural variability inferred from multicentennial paleoclimate records and the changes in rainfall patterns projected to occur in the coming century.

This paper estimates future prolonged drought risk using information from instrumental records, paleoclimate archives, and climate model simulations in simple Monte Carlo realizations of hydroclimate. The motivation for doing so comes from our notion of risk as a fractional quantity referring to the likelihood of prolonged drought occurrence. We rely on global climate model simulations of change during the twenty-first century as estimates of mean conditions in the future, and we use simple statistical models to build up large ensembles for calculating risk. This technique assumes the following:

1) Coupled global climate model simulations of the twenty-first century present a realistic view of the direction, magnitude, and uncertainty in forced precipitation changes, relative to today.
2) Paleoclimate records and observational data can empirically describe the distribution of variance across the frequency spectrum from interannual to multidecadal time scales in regional hydroclimate.
3) Simple models of time series are adequate for simulating the *local* statistical characteristics of hydroclimate across interannual to multidecadal time scales, regardless of whether these characteristics are externally forced or internally generated.

Justifications for statements 1 and 2 are straightforward: state-of-the-art models agree that semiarid subtropical regions throughout the world will tend to dry under climate change (e.g., Diffenbaugh and Giorgi 2012), and paleoclimate records, especially tree rings, are reasonably well validated and widely used to characterize variations of the past for a wide range of water resource management applications (Meko et al. 2012).

Assumption 3 in the list above deserves further elaboration. We begin by noting that in western North America over the last millennium, stochastic variability and autocorrelation alone may account for the magnitude of hydroclimatic variations on time scales from years to decades (Hunt 2011; Ault et al. 2013; Coats et al. 2013b). Second, one can easily imagine a situation where in a single realization of a given model, climatic forcing enhances overall aridity, but megadroughts do not occur because a few intermittent wet years disrupt their duration. Given the statistics of this model, megadroughts might still be likely, but would not be found in this particular realization.

The scenario delineated above is shown schematically in Fig. 1. Here, an idealized time series of some hydrological variable (say $P - E$) has been generated with unit variance and a mean of zero for the first 100 "years" (Fig. 1a). At year 101 the mean is shifted by -0.25σ and an additional 50 years of data are generated while the variance stays the same. Figures 1b and 1c show realizations of 50 yr of data with the same mean and variance as the final 50 yr of the series in Fig. 1a. Although both the time series in Figs. 1b and 1c have the same mean and variance, a prolonged period of time with low values (a "megadrought") is found in the first realization (Fig. 1b), whereas in the second realization (Fig. 1c) it is not.

Implied by Fig. 1 is the possibility that deterministic simulations of climate change using state-of-the-art numerical models may be insufficient for estimating megadrought risk because the ensemble sizes of such

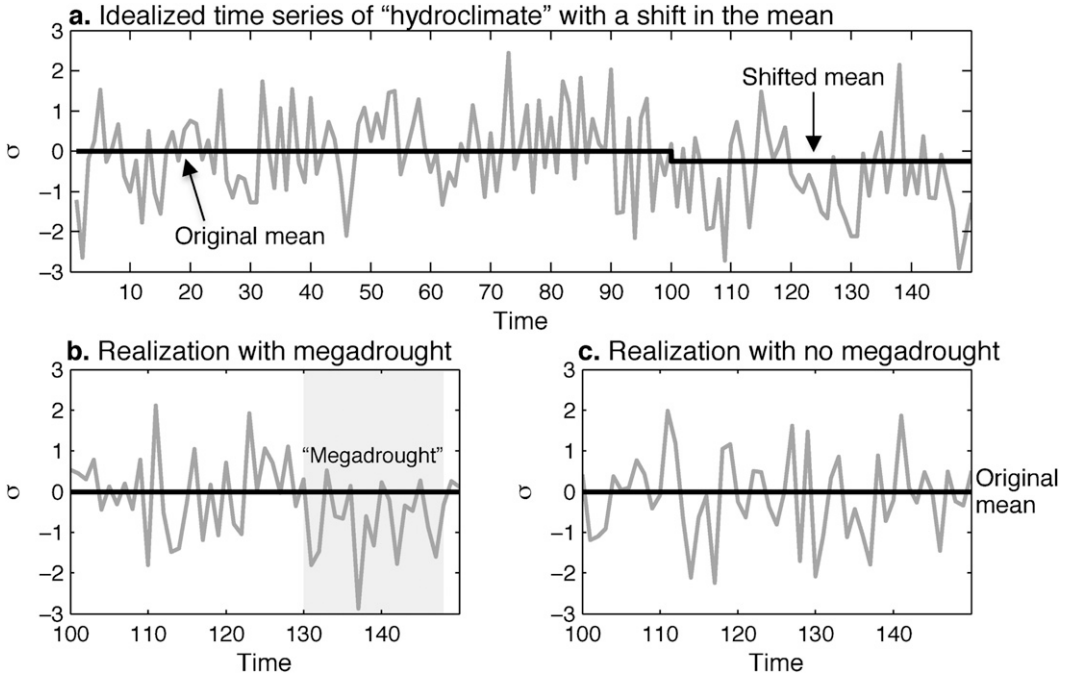

FIG. 1. Schematic illustration of why large ensembles are needed to calculate megadrought risk. (a) The black line shows the original and shifted mean, while (b),(c) the black lines show the original mean for reference. Importantly, the means and variances are the same for the final 50 yr in (a)–(c) but only the realization in (b) experiences a megadrought.

experiments are relatively small (tens of realizations per model at most), and the statistics of infrequent events such as megadroughts might not be robust. Using a multimodel ensemble does not completely guard against this limitation because model simulations disagree on the expression of forced changes in hydroclimate at regional scales (e.g., Diffenbaugh and Giorgi 2012). Instead, we use large ensembles of stochastic variables to emulate the statistics of interannual to decadal variability, and output from global climate models to estimate how precipitation is expected to change this century. The limitations and possible implications of this assumption are discussed in section 4.

2. Data and methods

To establish benchmarks for decadal drought and multidecadal megadrought, we use instrumental precipitation data (Fig. 2; Mitchell and Jones 2005), and several recent reconstructions of hydroclimate including the Palmer drought severity index (PDSI) for the southwestern United States (Cook et al. 2004), Colorado River streamflow reconstructions (Meko et al. 2007), and drought from northern Mexico (Stahle et al. 2011) (Fig. 3). Although the reconstructions are precisely dated, they target different regions and aspects of hydroclimate and hence are not expected to agree with each other through time (and indeed they do not; Fig. 3). In addition to these observational datasets, we use output from 27 coupled general circulation models (GCMs) that are members of the Climate Model Intercomparison Project phase 5 (CMIP5) archive. Models were included if at least one unforced preindustrial control (piControl) and forced ''historical'' (late nineteenth and/or twentieth century) experiment were available, as well as forced climate change simulations for each of the following representative concentration pathways (RCPs; Moss et al. 2010): RCP2.6, RCP4.5, and RCP8.5. For illustrative purposes, the projected changes in mean precipitation are shown for the RCP8.5 scenario in Fig. 4 (cf. Fig. 2 of Diffenbaugh and Giorgi 2012). The number of available runs from each simulation considered here is reported in the legend of the figure. All model and instrumental data were annualized (January–December) prior to analysis, although our results are not sensitive to the months used for annualization.

a. Standardizing hydroclimate indicators

Here we develop a systematic approach to normalizing hydroclimate fluctuations so that they retain their essential meaning whether they originate from climate model simulations, observational datasets, or

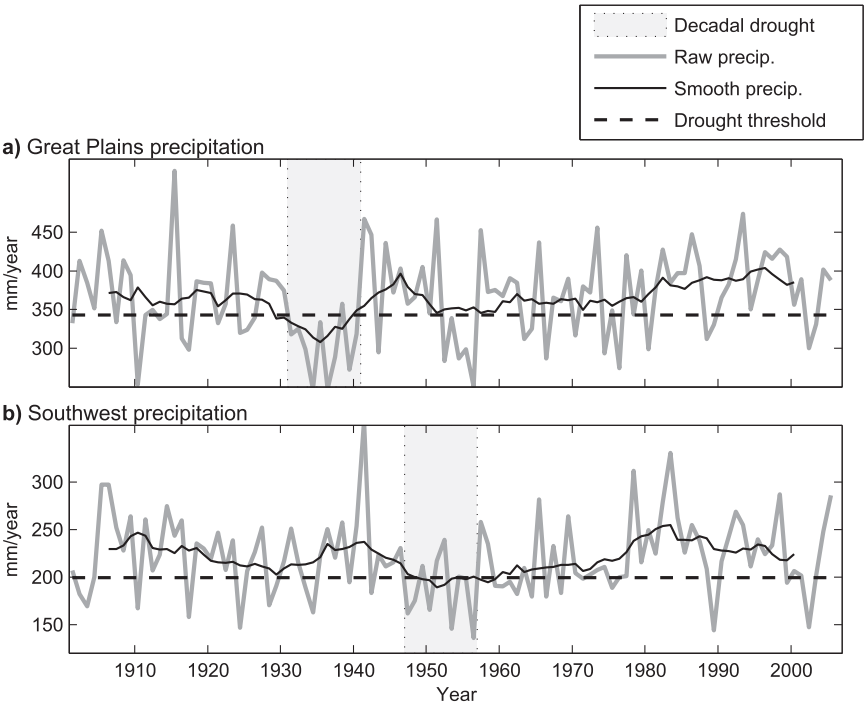

FIG. 2. The 11-yr running means of normalized paleoclimate reconstructions for twentieth-century precipitation data from (a) the U.S. Southwest and (b) the Great Plains. Precipitation data are from the University of East Anglia's Climate Research Unit's time series version 3.1 (TS3.1) dataset (Mitchell and Jones 2005). We identify decadal droughts as −0.5 standard deviations of raw data in the 11-yr mean (vertical gray bars).

paleoclimate reconstructions. We further seek to distinguish between decadal droughts, which have been experienced during the instrumental era (e.g., the 1930s Dust Bowl), and multidecadal megadrought events that are outside the range of variability experienced during the twentieth century. To begin, we consider two of the worst decade-scale droughts during the twentieth century: the 1930s Dust Bowl and the 1950s Southwest drought. Both of these intervals can be identified as -0.5σ departures in the decadal (11-yr) running mean of precipitation (Fig. 2).

Identifying -0.5σ events in the 11-yr means of paleoclimate records requires us to normalize these time series to exhibit unit variance over the twentieth century, so that fluctuations in the past are scaled relative to this baseline period. To that end we represent the entire Colorado streamflow record as normalized departures $[\hat{Z}(t)]$ from the late twentieth-century mean:

$$\hat{Z}(t) = \frac{F(t) - \hat{\mu}}{\hat{\sigma}}, \tag{1}$$

where $F(t)$ is reconstructed flow and $\hat{\mu}$ and $\hat{\sigma}$ are the mean and standard deviation, respectively, of the annual data over the reference period of 1950–2000 CE. The time series of $\hat{Z}(t)$ is a modified z score of $F(t)$, and its values through time are shown in Fig. 3a. Identifying intervals of -0.5σ departures in the running 11-yr mean highlights the 1150s, as well as several other low-flow decades, which occur about once per century (gray vertical bars). Time series from other recent drought studies (Cook et al. 2004; Stahle et al. 2011), normalized in the same way, are also shown in Figs. 3b and 3c. They suggest that the preindustrial rate of comparable decade-long droughts is ~1.5% century^{-1}, which is quite consistent with the literature-based estimate of 1%–2% century^{-1} of Woodhouse and Overpeck (1998).

Our definition of decadal drought captures major intervals of aridity during the twentieth century as well as others during the last millennium (Figs. 3 and 2). We employ a second and more stringent criterion to identify multidecadal megadrought. In this case, -0.5σ departures in the 35-yr mean are identified. Although this definition is somewhat arbitrary, it is useful because the thresholds employed are both longer in time and greater in magnitude than the descriptions of Meko et al. (2007) and Cook et al. (2007) used to characterize the worst droughts of the past millennium in Colorado streamflow and continental-scale hydroclimate, respectively. By setting the criterion for multidecadal megadrought

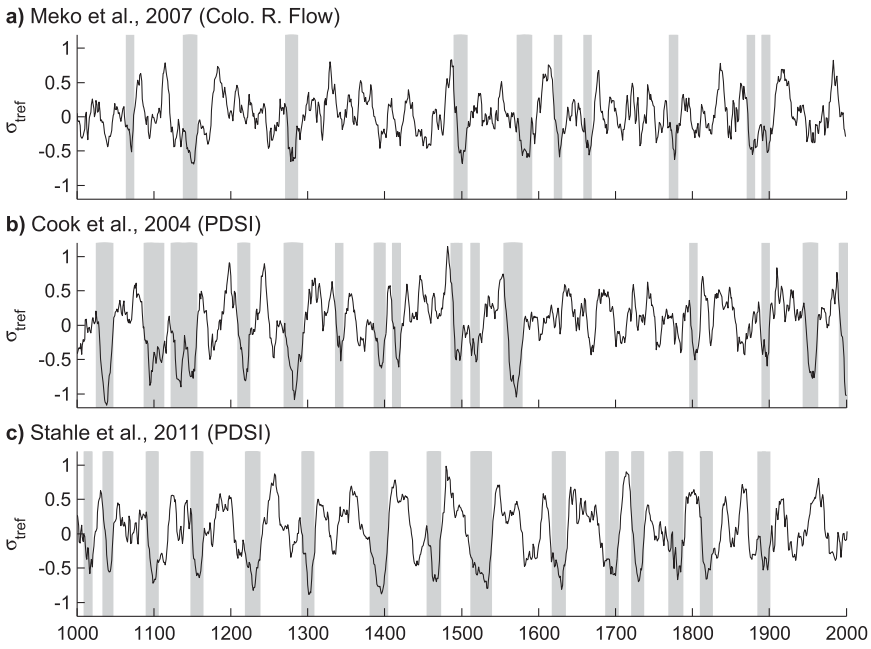

FIG. 3. The 11-yr running means of normalized paleoclimate reconstructions for (a) the Colorado streamflow (Meko et al. 2007), (b) reconstructed PDSI from the southwestern United States (Cook et al. 2004), and (c) reconstructed PDSI from Mexico (Stahle et al. 2011). Vertical gray bars indicate decadal-scale drought (a -0.5σ deviation in the 11-yr mean). All time series are standardized to exhibit one unit of standard deviation and a mean of zero over the 1950–2000 reference period.

beyond anything experienced during the last millennium, we suggest that our results will be insightful for developing adaptation and mitigation strategies for addressing worst-case scenarios. We also note that a 35-yr, -0.5σ event would be on par with the consequential late twentieth-century Sahel drought (e.g., Hoerling et al. 2006). Other similar thresholds (e.g., 25 or 45 yr) would produce qualitatively similar spatial patterns, but the rates of megadrought occurrence and levels of megadrought risk would of course differ from the ones we report here. In particular, for a given magnitude (say -0.5σ) the risk of shorter events would be higher and the risk of longer events would be lower than that for a 35-yr event.

b. *Monte Carlo simulations of drought*

With the definitions of "decadal drought" (an 11-yr, -0.5σ event) and "multidecadal megadrought" (a 35-yr, -0.5σ event) that we have outlined above, we now develop "null" expectations for the rate at which these events would occur from random chance under a stationary climate, but with three different assumptions about the underlying frequency characteristics of hydroclimate variability on interannual to centennial time scales.

We begin by examining the statistics of prolonged drought when interannual hydroclimate fluctuations are simulated as normally distributed white noise with unit variance and standard deviation. An example of one such time series, $X_w(t)$ is shown in Fig. 5. The decadal drought statistics of this type of noise, obtained from 1000 white noise realizations (each of length 100 years), are summarized in Fig. 6. If the distribution of variance across the hydroclimatic continuum were indeed white, then decadal droughts would be expected to occur at a rate of slightly $<1\,(100\,\mathrm{yr})^{-1}$ (Fig. 6a), and the risk of such an event occurring during any given 50-yr period would be around 45% (Fig. 6b). The likelihood of a multidecadal megadrought during any given 50-yr period would be only about 0.45% (Fig. 6b). This preliminary Monte Carlo result establishes a benchmark for the minimum rate at which decadal droughts and megadroughts would occur in a climate with only stochastic interannual variability and no sources of long-term persistence.

Although raw precipitation tends to have a white spectrum on interannual time scales (e.g., Vasseur and Yodzis 2004; Ault and St George 2010), the underlying continuum of hydroclimate may be somewhat "redder" in WNA (Cayan et al. 1998; Ault and St George 2010; Ault et al. 2012, 2013). Moreover, drought indices typically have a source of built-in autocorrelation to accommodate the reality that surface moisture stores

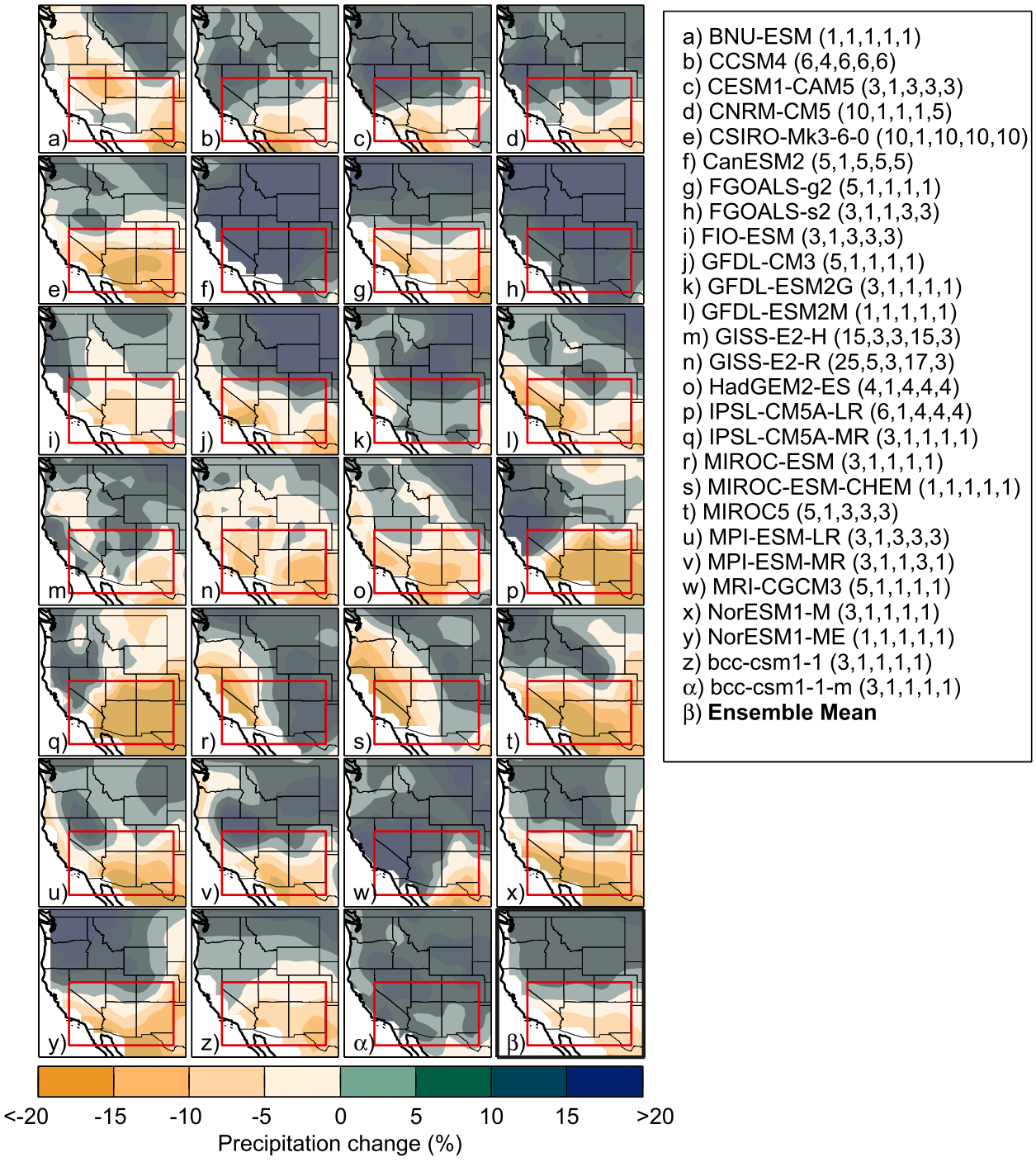

FIG. 4. Map of projected precipitation over the twenty-first-century (2005–2100) change in the RCP8.5 scenario shown as a percentage of twentieth-century precipitation change [as in the global maps of Diffenbaugh and Giorgi (2012)]. For each model, the number of available runs from each experiment is shown in parentheses in the following order: historical, piControl, RCP2.6, RCP4.5, and RCP8.5. The red box shows the greater southwestern United States to emphasize the focus of this study (30°–40°N, 120°–103°W).

depend on their prior states (i.e., they have ''memory''). For example, PDSI models the surface water balance using a simplified approximation of soil moisture, and has a built-in autocorrelation function (e.g., Alley 1984; Wells et al. 2004). Similarly, the standardized precipitation index (SPI) integrates anomalies over a number of predefined lags to measure how aggregated rainfall anomalies deviate from their long-term averages.

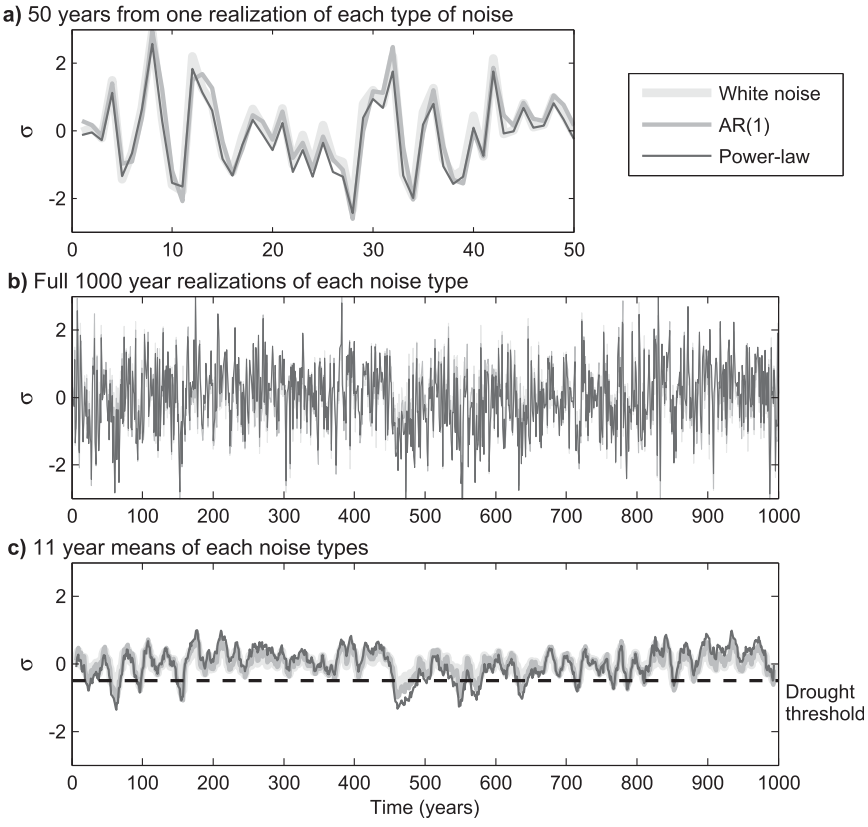

FIG. 5. Examples of Monte Carlo (MC) time series used to simulate decadal drought with three different underlying frequency characteristics [white noise, AR(1), and power law]: (a) 50 yr of a single MC realization of each type of noise, (b) the 1000-yr full realization of each noise type, and (c) the 11-yr running mean of each type of noise, shown with the dashed line denoting a decadal drought (e.g., a -0.5σ in the 11-yr running mean). Importantly, each MC time series has a mean of zero and unit standard deviation, and differ only in the distribution of their variances across the power spectrum. Moreover, the AR(1) and power-law time series are generated by rescaling the white noise data, which is why the different realizations of noise appear so strongly correlated with each other.

In a simplistic sense, year-to-year persistence can be described as a first-order autoregressive [AR(1)] process [$X_{\mathrm{AR}(1)}(t)$]:

$$X_{\mathrm{AR}(1)}(t) = \alpha X_{\mathrm{AR}(1)}(t-1) + X_w(t), \qquad (2)$$

where α is the lag-1 (i.e., 1 yr) autocorrelation coefficient and is derived empirically from data, $X_{\mathrm{AR}(1)}(t)$ is autoregressive red noise, and $X_w(t)$ is the white noise input. In WNA, the value of α is about 0.3 on interannual time scales for the three (tree ring based) paleoclimate reconstructions shown in Fig. 3, as well as for many other hydroclimate indicators (Ault et al. 2013). A single realization of this type of noise (normalized to exhibit unit variance overall) is shown in Fig. 5, and the statistical characteristics of megadroughts in this type of noise are shown in Fig. 6.

Despite the intuitive and simple representation of hydroclimate as an AR(1) process—moisture deficits tend to persist through time—there is some evidence that such an approximation misses key characteristics of variability on longer time scales (Pelletier and Turcotte 1997; Kantelhardt et al. 2006; Koscielny-Bunde et al. 2006; Ault et al. 2013). As a complementary approach, we also simulate hydroclimate as a process with underlying frequency characteristics that are described by a weak power-law relationship between frequency f and variance $S(f)$, such that $S(f) \propto f^{-\beta}$. Power spectra with higher values of β correspond to time series that exhibit more variance at lower frequencies. To generate time series with this type of frequency behavior, we employ a method similar to the one described by Pelletier and Turcotte (1997) and explained thoroughly in Pelletier (2008). First, we calculate the discrete Fourier transform of

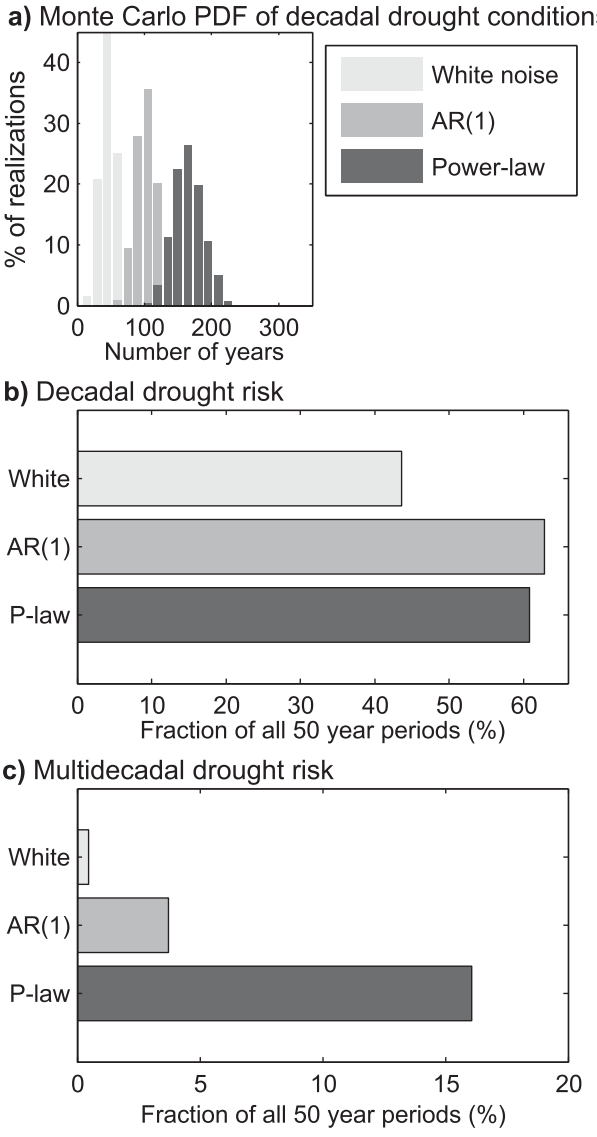

FIG. 6. Statistics summarizing Monte Carlo simulations: (a) distributions of years spent in decadal (≥11 yr) drought conditions for each type of noise (as a percentage of all realizations), (b) risk of *at least* one decadal (≥11 yr) drought during any given 50-yr window in any realizations, and (c) risk of a multidecadal (≥35 yr) drought during any 50-yr window. Risk in (b) and (c) is expressed as a percentage of the total number of simulations.

a white noise time series $X_w(t)$, and filter it to conform to a predefined value of β:

$$\tilde{X}_p(k) = \psi_k \sum_{t=1}^{N} X_w(t) e^{-i2\pi k[(t-1)/N]}, \quad k = 0, \ldots, N-1, \tag{3}$$

where k are the standard Fourier frequencies and N is the length of the time series. The term ψ_k rescales the Fourier coefficients so that they are approximately power-law distributed:

$$\psi_k = \begin{cases} \left(\frac{1}{N}\right)^{-\beta/\sqrt{2}} & \text{if} \quad k = 0 \\ \left(\frac{k}{N}\right)^{-\beta/\sqrt{2}} & \text{otherwise}. \end{cases} \tag{4}$$

Here the value of β is divided by $\sqrt{2}$ because it is being applied to the raw Fourier coefficients, which have amplitudes proportional to the square root of the power spectrum.

The rescaled Fourier series $\tilde{X}_p(k)$ is then used to generate power-law time series $X_p(t)$ by taking the real part of the inverse Fourier transform of $\tilde{X}_p(k)$:

$$X_p(t) = \mathrm{Re}\left\{\frac{1}{N}\sum_{k=0}^{N-1} \tilde{X}_p(k) e^{-i2\pi k[(t-1)/N]}\right\}, \quad t = 1, \ldots, N. \tag{5}$$

Finally, the mean and variance are restored to the values of the original white noise data (zero and unity, in this case).

We used a value of 0.5 for β to rescale each realization of $X_w(t)$, which was suggested as an appropriate estimate by Ault et al. (2013) from synthesis of tree-ring reconstructions of precipitation, PDSI, and streamflow as well as non-tree-ring estimates of hydroclimate. As a check, we calculated the power laws of the noises after they had been rescaled. We found that the actual values of β varied from one realization to the next, but were generally between 0.4 and 0.6. This range agrees well with instrumental and paleoclimate estimates of this parameter for the region, and is certainly within the observational uncertainty (Ault et al. 2013). Importantly, time series with spectra scaled by power laws of ~0.5 will also appear to exhibit autocorrelation of about 0.3, which in turn implies that the AR(1) and power-law realizations will behave very similarly on short time scales, but not necessarily on longer ones (e.g., Pelletier and Turcotte 1997; Ault et al. 2013). Finally, our use of power-law noises does not make any assumptions about the underlying climate dynamics governing the shape of the power spectrum of hydroclimate: linear and nonlinear processes alike may produce such spectral distributions (Milotti 1995; Penland and Sardeshmukh 2012).

Table 1 highlights a few key features of the two models employed here. In particular, the noise models used to estimate drought risk use parameters that do not vary across space, and all are scaled to the twentieth-century mean and variance. The autocorrelation parameter of 0.3 is a middle-of-the-road value from the time series

TABLE 1. Summary of the two red noise models used here to estimate drought risk in western North America. The key parameters are reported in the second column, and they do not vary spatially. The value of α (0.3) is the approximate autocorrelation of the three time series in Fig. 3, as well as the data analyzed in (Ault et al. 2013, Fig. 2), which supports values between 0.25 and 0.35. The estimate used for β (0.5) is a middle-of-the-road estimate from those reported in (Ault et al. 2013), and also Fig. 7.

Model	Parameters	Estimated from	References
AR(1)	α(0.3)	Streamflow, soil moisture, tree-ring reconstructions	Meko et al. (2007); Cook et al. (2004); Stahle et al. (2011); Ault et al. (2013); this study
Power law	β(0.5)	Long tree-ring chronologies, other hydroclimate proxies	Pelletier and Turcotte (1997); Ault et al. (2013); this study

shown in Fig. 3, and is well within the range of estimates for autocorrelation in the region from other paleoclimate and observational datasets (Ault et al. 2013). The value used for β (0.5) is from the analysis of proxy records in Ault et al. (2013) as well, and is supported by Fig. 7.

Sample time series and statistics of power-law realizations of drought (Figs. 5 and 6, respectively) reveal the importance of low-frequency variability in shaping prolonged drought risk. Over the time scale of 50 years, the white, AR(1), and power-law noises are all remarkably similar to each other [because the initial realization of $X_w(t)$ is rescaled to produce both $X_{\mathrm{AR}(1)}(t)$ and $X_p(t)$]. On the time scale of a millennium (Fig. 5b), the low-frequency differences are more apparent. The running 11-yr mean of each noise type (Fig. 5b) makes the implications for risk clear: the AR(1) and power-law time series spend more time in drought and depict higher levels of risk for megadrought. In Fig. 6a, it is also clear that the fraction of time spent in decadal drought conditions is about 17% for the power-law noise realizations, as opposed to 10% for the AR(1) simulations, and less than 5% for the white noise time series. Although the AR(1) and power-law time series exhibit similar likelihoods that a single decadal drought will occur during any given 50-yr period, the power-law series yields events that persist for longer. Drought risk on longer time scales, however, is clearly far higher for the power-law distributed time series than for the other two, with the risk of a 35-yr (-0.5σ) megadrought being greater than 16% for any given 50-yr segment. We stress that these risks apply to a stationary climate with no local feedbacks or externally forced changes. They are therefore our most conservative baseline estimates of prolonged drought risk during the coming century.

c. *Projected risk of persistent drought in CMIP5 simulations*

Our definition of megadrought is easily extended to climate model data. For instance, projected precipitation at the jth position of each grid of a given model can be transformed as

$$\hat{Z}_j(t) = \frac{P_j(t) - \hat{\mu}_j}{\hat{\sigma}_j}, \tag{6}$$

where $\hat{\mu}_j$ and $\hat{\sigma}_j$ are the late twentieth-century (1950–2000 CE) mean and standard deviation, respectively. The subscript j is used as a spatial index (i.e., a point on a grid).

Certain limitations make estimating megadrought risk in the CMIP5 archive more complicated than simply

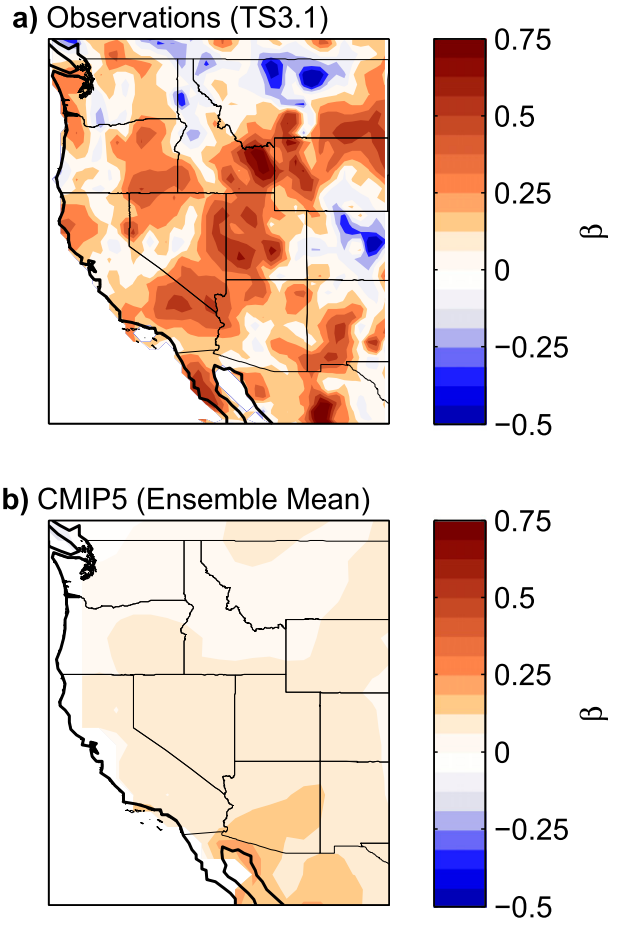

FIG. 7. Power-law estimates (β) from (a) twentieth-century instrumental data and (b) and CMIP5 historical (1850–2005 CE) simulations. Instrumental data originate from the University of East Anglia's TS3.1 data product and, like the CMIP5 records, were annualized prior to calculating β.

calculating how often these events occur in climate projections. First, the number of ensemble members available from each model is small (Fig. 4), and the role for internal variability may be substantial on decadal to multidecadal time scales (Hawkins and Sutton 2009; Deser et al. 2012). This makes it difficult to reliably estimate risks stemming from the combined influences of forced changes and internal variability. Second, the distribution of variance across time scales is different in observational data than in models. In particular, models tend to exhibit power spectra resembling white noise in WNA, even when run for many centuries or forced with the time-evolving boundary conditions of the last millennium (Ault et al. 2012, 2013). To illustrate this point further here, we show power-law estimates from observations and CMIP5 data in Fig. 7. In this case, the power-law coefficients are calculated from each model individually and then averaged together to produce this map. Importantly, the results of individual models appear similar to this ensemble average, supporting recent findings that the continuum of hydroclimate in WNA appears to be considerably redder in observations than in models (Ault et al. 2013, 2012).

We address the aforementioned challenges by developing a Monte Carlo model of hydroclimate variability to emulate the statistics of both natural variability and climate change in WNA. This approach enables us to evaluate projected risk of prolonged drought in the twenty-first century for a given climate change scenario. We use the underlying frequency characteristics of observational data (including paleodata), as well as projected changes in precipitation simulated by models archived as part of CMIP5. The Monte Carlo model is described by

$$\hat{Z}_{ij}(t) = X_w(t)\left(\frac{\hat{\varrho}_{ij}}{\hat{\sigma}_{ij}}\right) + \xi(\Delta\hat{\mu}_{ij}, \sigma^2_{\mu_{ij}}), \qquad (7)$$

where $\hat{Z}_{ij}(t)$ is normalized precipitation of the ith model at the jth point on a grid, and $X_w(t)$ is a normally distributed time series of white noise with unit variance. The quantity $\hat{\varrho}_{ij}/\hat{\sigma}_{ij}$ scales the white noise by normalizing the twenty-first-century standard deviations ($\hat{\varrho}_{ij}$) from a given model grid point by the corresponding twentieth-century reference standard deviation ($\hat{\sigma}_{ij}$). Twentieth- to twenty-first-century differences in mean precipitation at each point in each model are represented by the random, normally distributed variable ξ_{ij}, with expected mean of $\Delta\hat{\mu}_{ij}$ (the change in precipitation) and variance ($\sigma^2_{\mu_{ij}}$), estimated from ensembles of runs when possible, and otherwise set to zero. Finally, to generate Monte Carlo twenty-first-century realizations of hydroclimate with AR(1) and power-law distributions in frequency space, we rescale $\hat{Z}_{ij}(t)$ following the same methods described above.

We estimate decadal drought and multidecadal megadrought risk in three climate change scenarios (RCP2.6, RCP4.5, and RCP8.5) for each of the 27 CMIP5 models considered here by generating 1000 stochastic (white noise) realizations, each 1000 years long, of WNA hydroclimate using Eq. (7), as well as the AR(1) and power-law rescaling procedures. In each model, and for each RCP, estimates of $\hat{\sigma}$ are made using the 1950–2000 portion of the model's historical simulation, and $\hat{\varrho}$ is estimated over the 50-yr interval spanning 2050–2100. Likewise, $\Delta\hat{\mu}$ and σ^2_{μ}, are estimated from the differences between historical (1950–2000) and late twenty-first-century (2050–2100) precipitation means. We then identify the percentage of all 1000 realizations that experience decadal drought or multidecadal megadrought conditions in each RCP, model, and type of noise.

3. Results

In the CMIP5 control runs, rates of decadal drought occurrence (the average number of events per century) are spatially uniform and close to one (Fig. 8a). Similarly, white noise realizations also tend to produce about one event per century. Under climate change, rates of decadal drought occurrence show more regional diversity than in the controls (Figs. 8b–d). In the northern part of WNA, rates are close to zero, whereas throughout much of the U.S. Southwest they are between 1.5 and 1.75. Multidecadal megadrought rates are close to zero in the control runs of the CMIP5 archive (Fig. 8e). Under climate change, these rates are closer to 0.5 (or 1 event per 200 yr), but they are still quite rare (Figs. 8f–h).

The risk of a single decade-long drought over any given 50-yr period in the control runs is about 50% (Fig. 9a), which is intuitive because the corresponding rate is about one per century. Decadal drought risk in the climate change scenarios, estimated over the period 2050–2100, depicts a decrease in the northern regions, and an increase to between 60% and 80% (Figs. 9b–d) in the U.S. Southwest. Moreover, risk increases in the U.S. Southwest with the intensity of the warming; the highest levels are found under the RCP8.5 scenario.

In the unforced control runs, the risk of a multidecadal megadrought is less than 1% throughout the region (Fig. 9e). Under climate change, however, risks in the U.S. Southwest increase to 10%–20% in RCP2.6 (Fig. 9f), 20%–40% in RCP4.5 (Fig. 9g), and 30%–50% in RCP8.5 (Fig. 9h).

A qualitatively similar picture of risk to that in Fig. 9 is seen in Figs. 10 and 11, which summarize our Monte

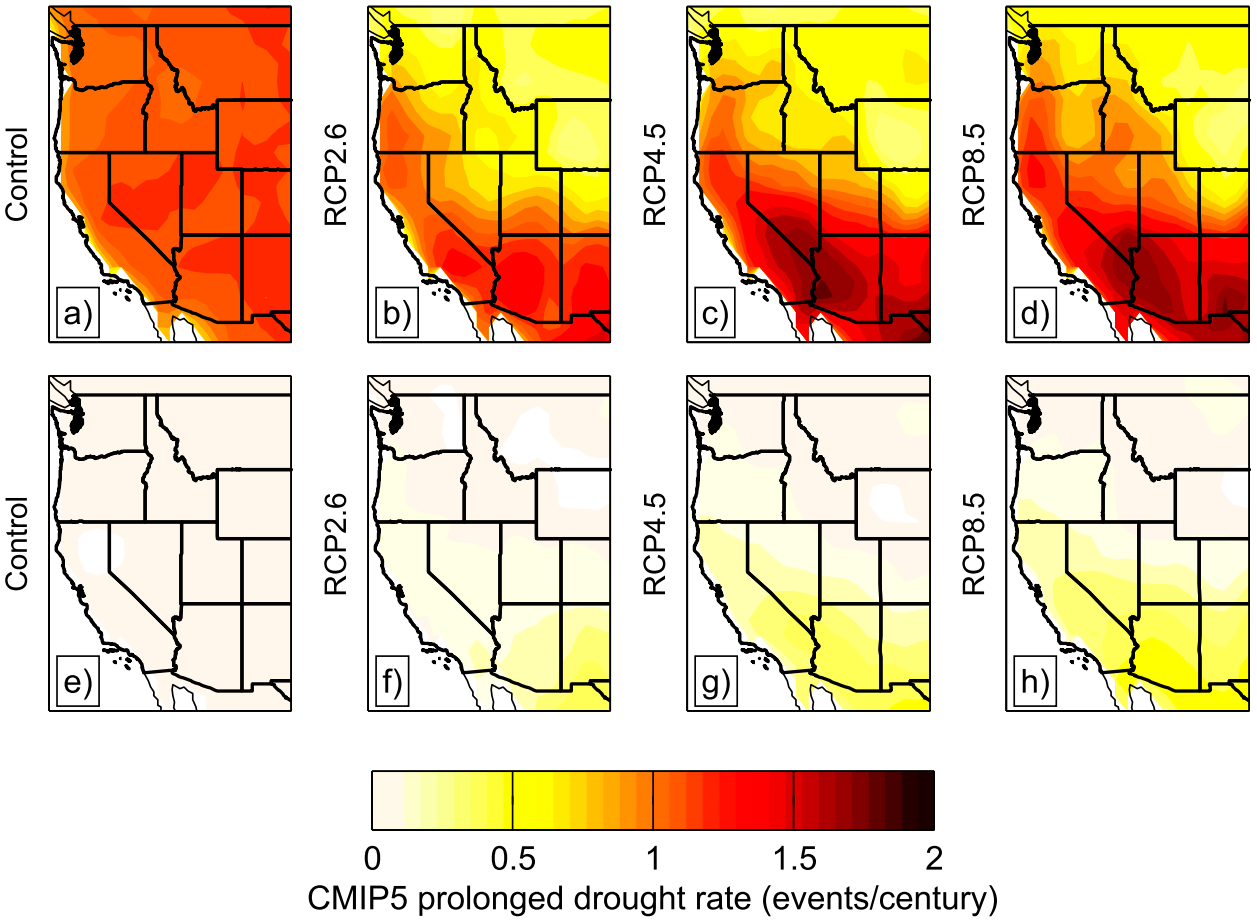

FIG. 8. Estimated rate of prolonged drought occurrence in (a),(e) control and (b)–(d),(f)–(h) forced CMIP5 simulations. The rate is calculated as the number of events per century averaged across all models, and across all centuries in the control cases in (a) and (e). (top) Indicates the rate of decadal (≥11 yr) drought, and (bottom) the rate of multidecadal (≥35 yr) megadrought occurrence. Forcing scenarios are indicated to the left of each map.

Carlo experiments using Eq. (7) to generate stochastic hydroclimate realizations, and the procedures described in section 2b to rescale them to exhibit AR(1) and power-law frequency distributions. In the U.S. Southwest, for example, risk of droughts at both decadal and multidecadal time scales increases with the intensity of the greenhouse gas forcing (columns) and type of noise (rows). Uncertainty in our risk estimates is depicted by the standard deviations of the individual model estimates of risk in Fig. 12. Results for the multidecadal megadrought risk standard deviations are shown in Fig. 13.

Thus far, we have only considered the risk of a prolonged period of aridity using two somewhat narrow definitions of decadal drought and megadrought. To develop a more complete representation of drought risk across a wide range of time scales and magnitudes, we examine the two-dimensional probability density function of drought risk using the same time scale-independent definition employed by Ault et al. (2013). Specifically, a drought is defined as a period of time during which $^{3}/_{5}$ of the antecedent years are below a particular threshold. These thresholds are the values of the x axes on the individual panels of Fig. 14, and the time scales are shown on the y axes of that figure. As in the earlier figures, risk is estimated from all Monte Carlo simulations of each model for each RCP, then averaged across the individual CMIP5 members to produce the ''magnitude versus duration'' diagrams in Fig. 14.

The results in Fig. 14 show that risk increases with GHG forcing intensity across all time scales in the raw CMIP5 archive (Figs. 14a–c), as well as for each type of noise. It also illustrates that the AR(1) and power-law distributions depict higher levels of risk on decadal and longer time scales than the white noise and CMIP5 ensembles. To emphasize this point further, we show the differences in drought risk across time scales between each type of noise and the raw CMIP5 estimates in Fig. 15. From this figure, it is clear that the low-probability (but

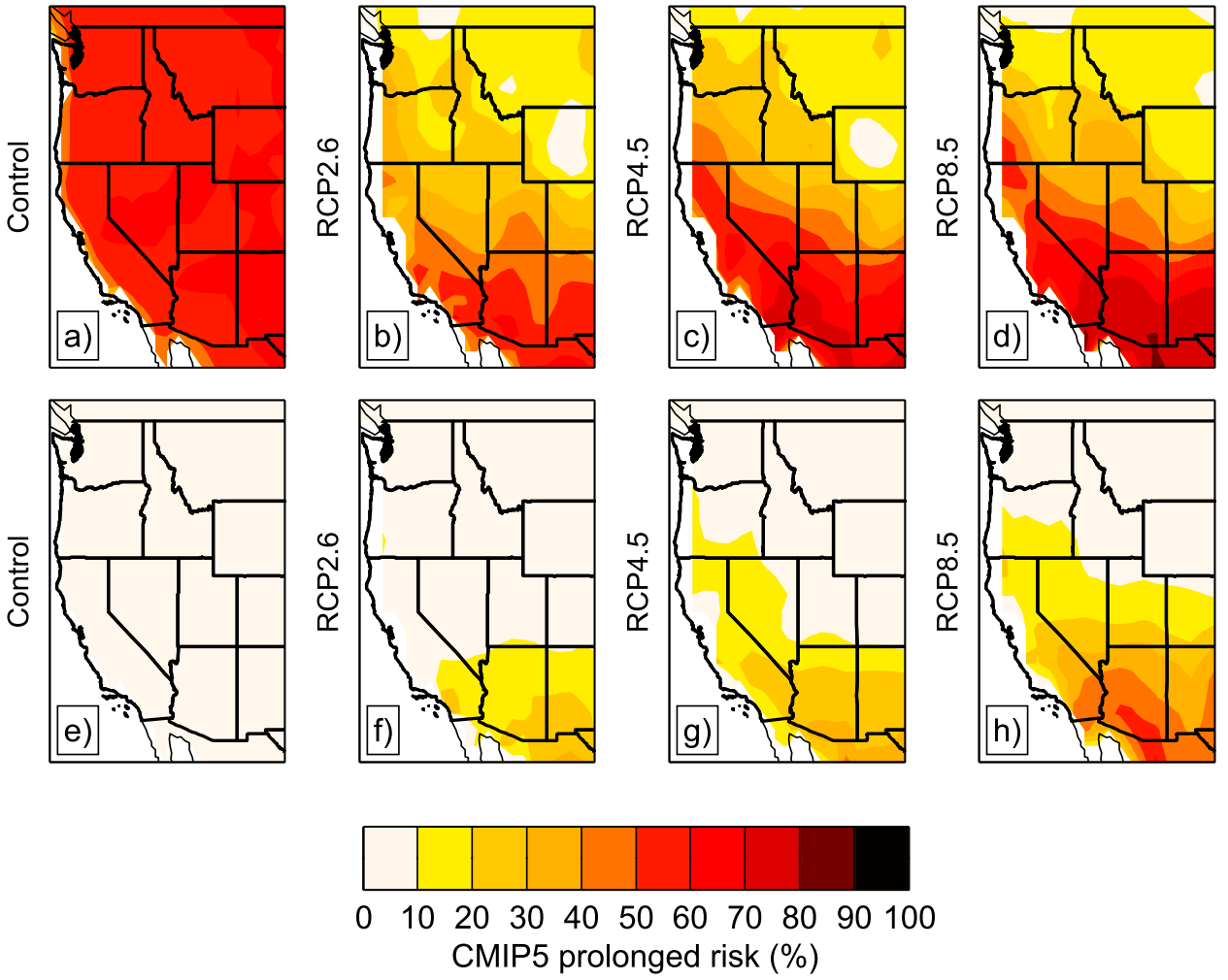

FIG. 9. Estimated risk of at least one prolonged drought in (a),(e) control and (b)–(d),(f)–(h) simulations. (top) Indicates the risk of decadal (>11 yr) drought, and (bottom) indicates the risk of multidecadal (>35 yr) megadrought. The risk is calculated as the percent of the total number of models (27) that simulate decadal or multidecadal megadrought. Forcing scenarios are indicated to the left of each map.

presumably consequential) "tails" of the distributions are far more likely in the AR(1) and power-law noises than in the raw CMIP5 archive. For instance, under the RCP8.5 scenario, the risk of a 0.5σ event on 40-yr time scales is below 5% as estimated from CMIP5 runs (Fig. 14c), but closer to 10% in the power-law noise realizations (Fig. 14i).

We extend our analysis of megadrought risk in the western United States to the rest of the world by examining raw CMIP5 estimates of decadal drought and multidecadal megadrought from the three RCP scenarios (Fig. 16). Risks throughout the subtropics appear as high as or higher than our estimates for the U.S. Southwest (e.g., in the Mediterranean region, western and southern Africa, Australia, and much of South America). We do not attempt to develop regionally appropriate stochastic realizations of precipitation at this time, although such an endeavor could be straightforward in areas where instrumental and paleoclimate data are adequate to characterize the underlying continuum of hydroclimate. In areas where low-frequency variability in precipitation is substantial and not well simulated by climate models (e.g., West Africa; Ault et al. 2012), the results shown here likely underestimate future risk of persistent drought.

We stress that our results have only used precipitation, yet temperature may play a substantial role in driving or exacerbating drought. Also, we used the low end of β estimates from Ault et al. (2013) to generate the power-law noises, but higher values might be realistic on long time scales, according to the preponderance of paleoclimate evidence considered in that study, and would raise the levels of risk. Hence, to the extent that the global climate models simulate future change realistically and

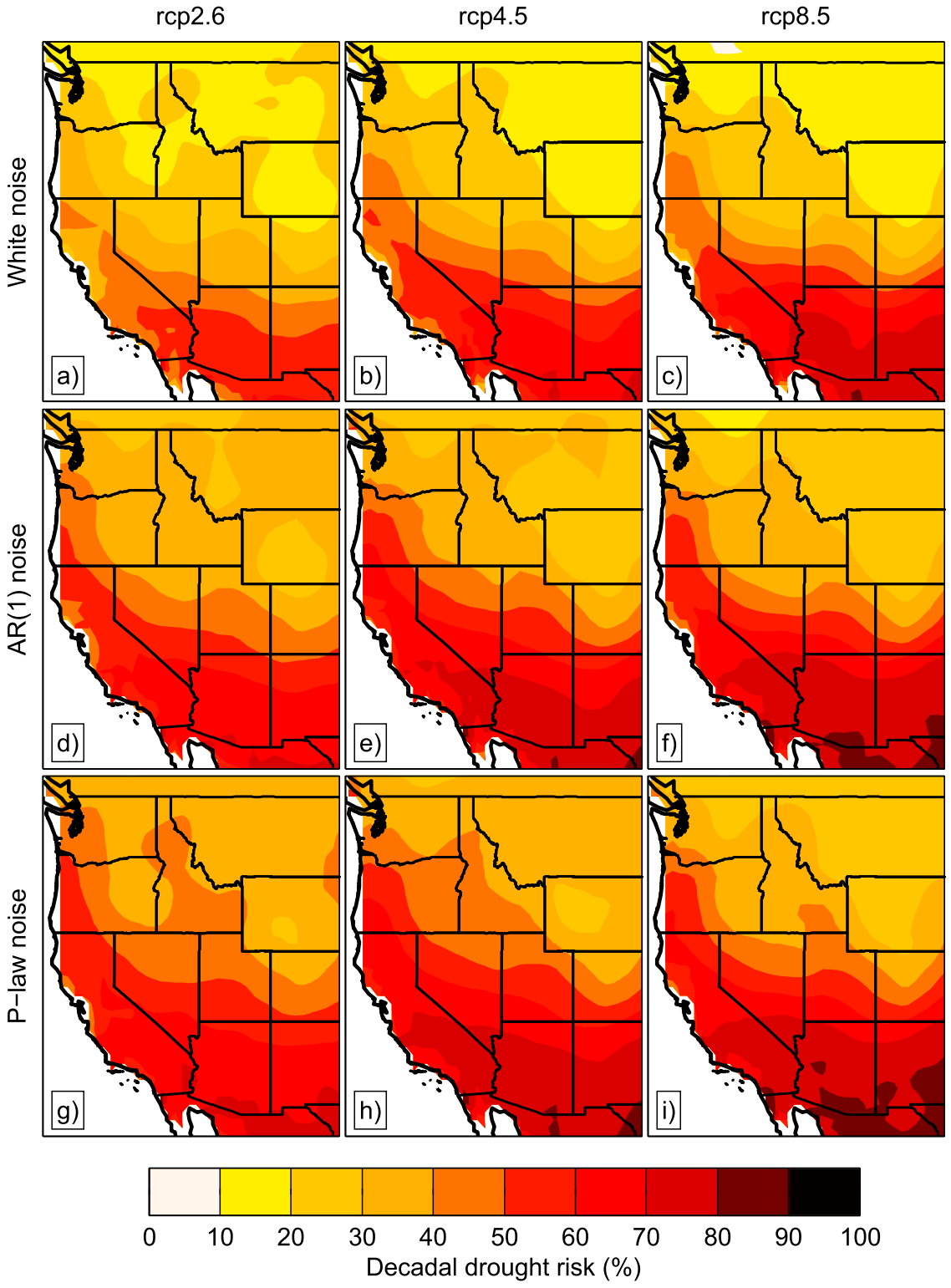

FIG. 10. Decadal (>11 yr) drought risk estimates obtained from Monte Carlo simulations of projected precipitation changes across all models in three different climate change scenarios (columns) and for three different types of noises (rows). These maps express the average risk estimates obtained from Monte Carlo simulations of precipitation in each model under three climate change scenarios. For each of the 27 individual CMIP5 models, risk is calculated as the percentage of the total number of Monte Carlo simulations (1000) that show a decadal drought. Here, those estimates of risk are averaged across the multimodel archive.

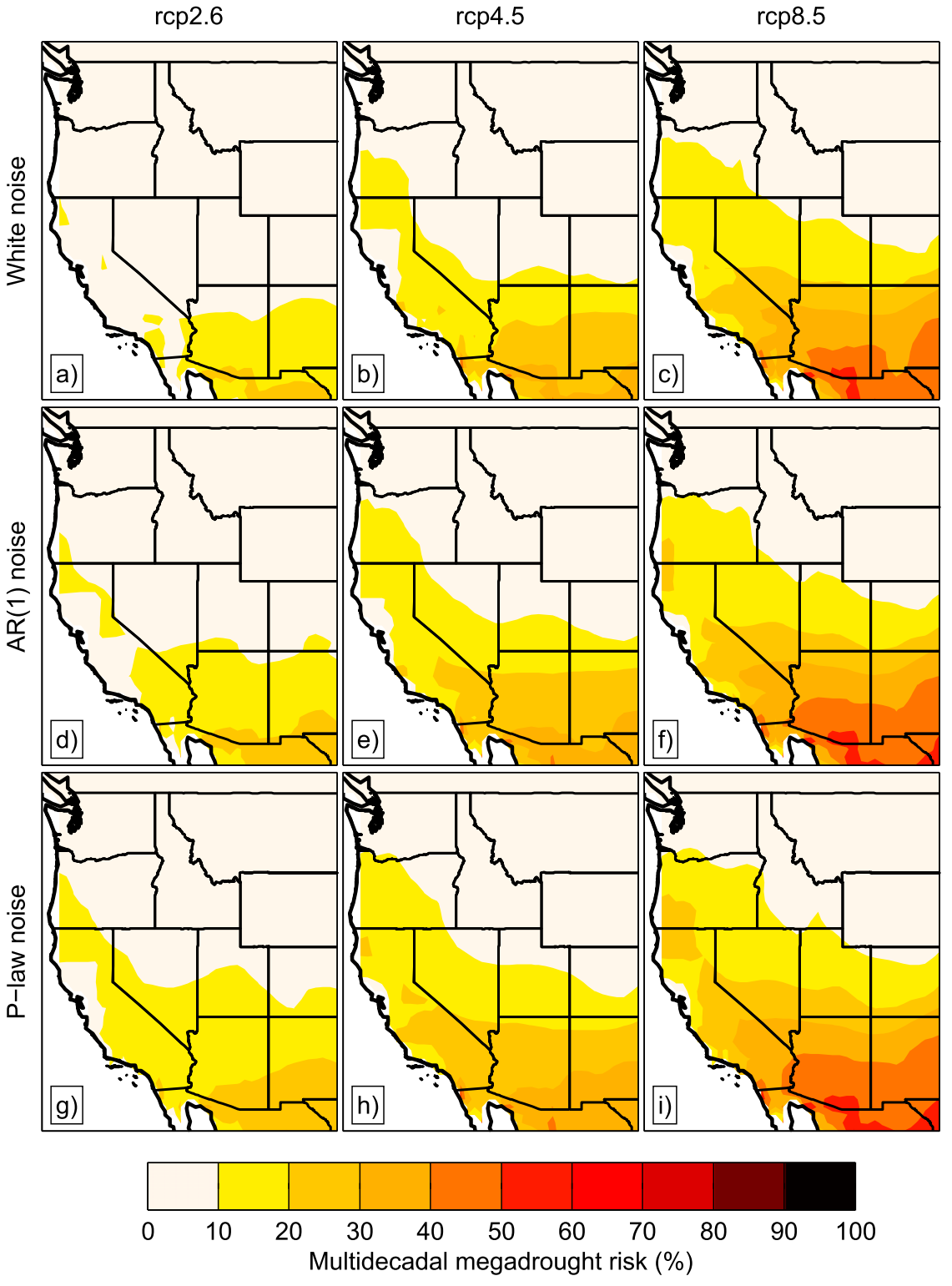

FIG. 11. Multidecadal (>35 yr) megadrought risk estimates obtained from Monte Carlo simulations of projected precipitation changes across all 27 CMIP5 models in three different climate change scenarios (columns) and for three different types of noises (rows). These maps express the average risk estimates obtained from Monte Carlo simulations of precipitation in each model under three climate change scenarios. For each of the 27 individual CMIP5 models, risk is calculated as the percentage of the total number of Monte Carlo simulations (1000) that show a multidecadal megadrought. Here, those estimates of risk are averaged across the multimodel archive.

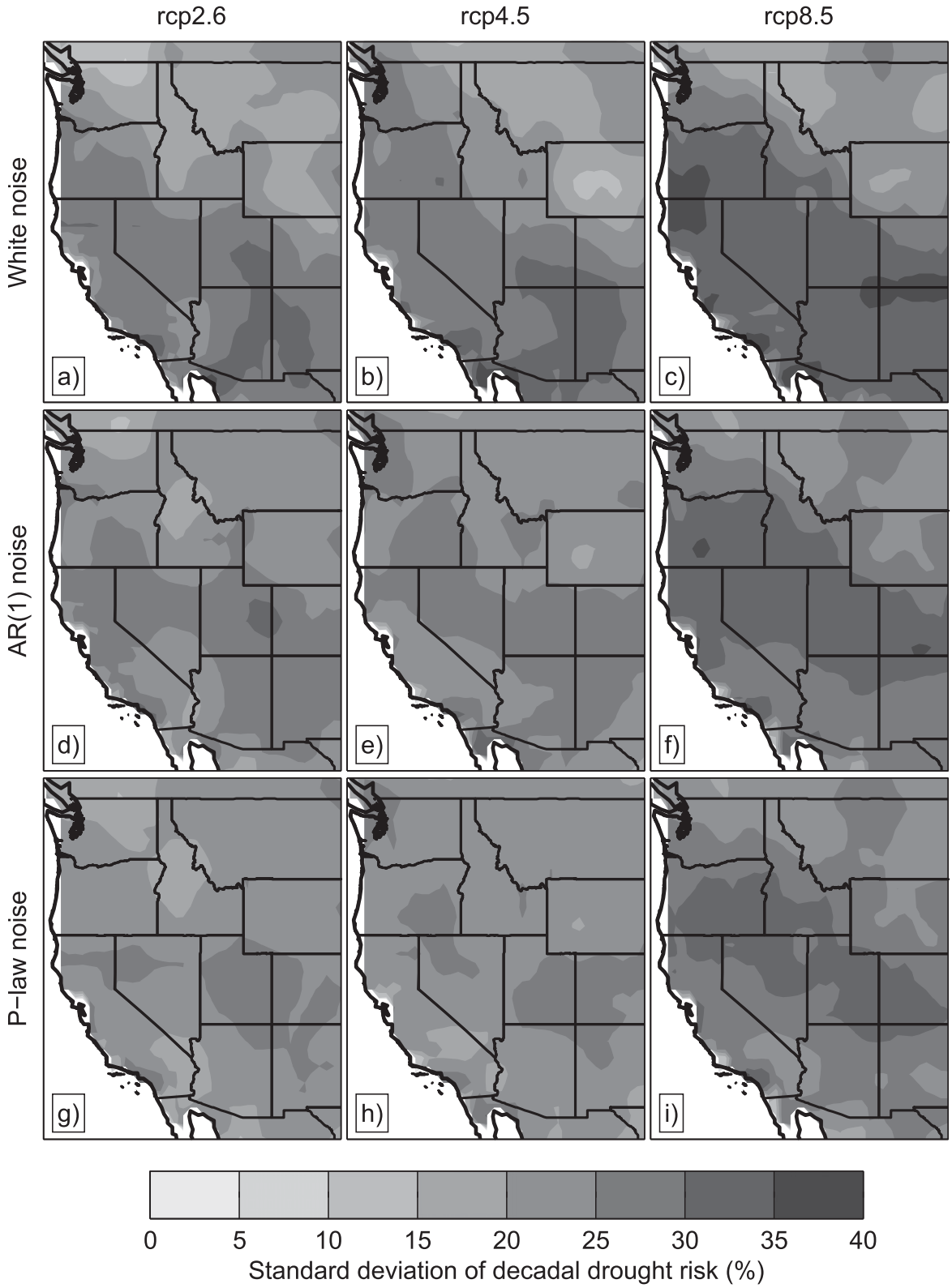

FIG. 12. Standard deviations of decadal (>11 yr) drought risk estimates in Fig. 10. Standard deviations are calculated from the individual risk estimates of each model at each point for three different climate change scenarios (columns) and for three different types of noises (rows). These maps express the spatial variability of uncertainty in the risk estimates of Fig. 10.

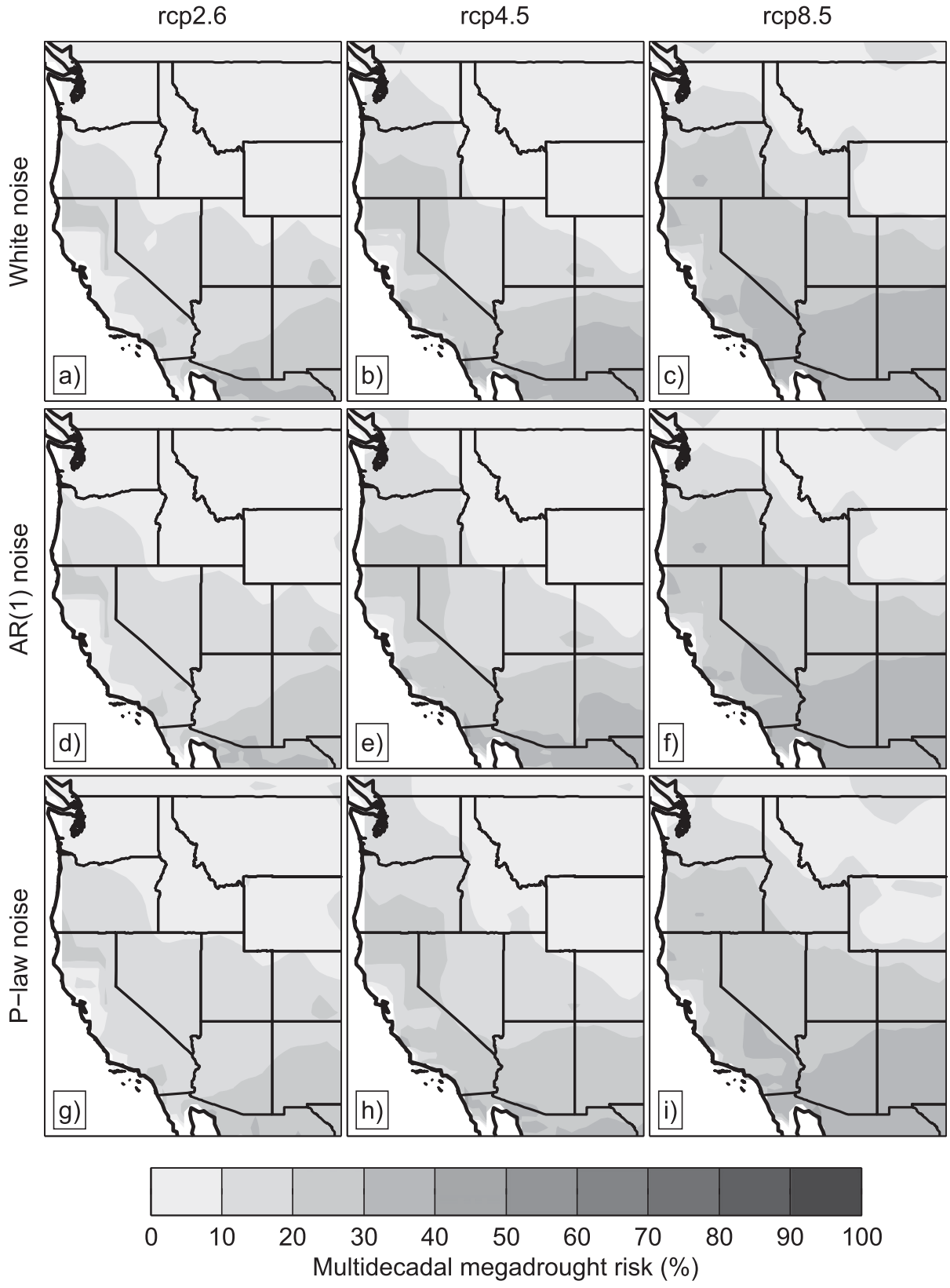

FIG. 13. Standard deviations of drought risk estimates as in Fig. 12, but for multidecadal (>35 yr) megadrought risk.

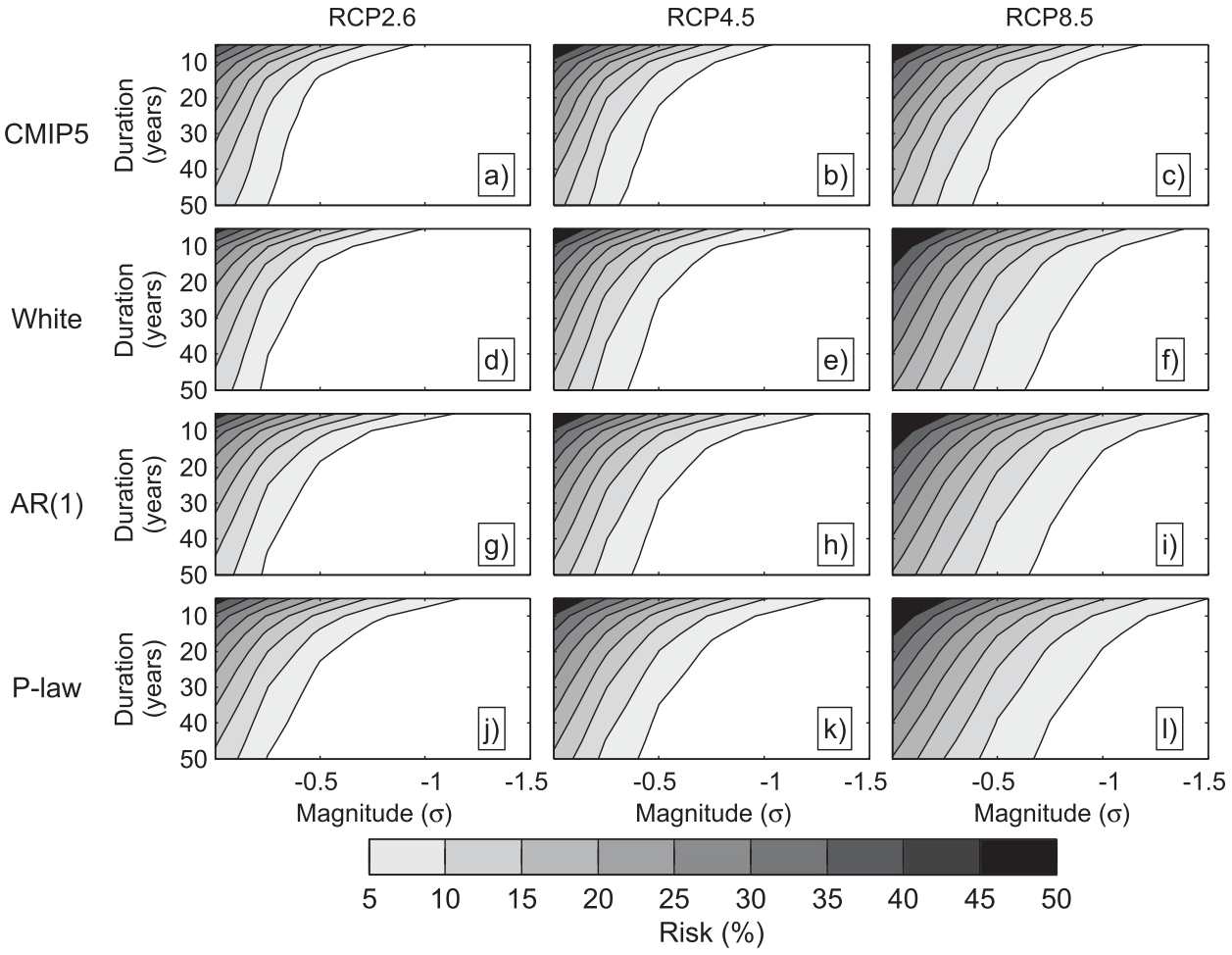

FIG. 14. Drought magnitude vs duration for realizations of southwestern U.S. precipitation time series in each climate change scenario, obtained from the following sources: (a)–(c) raw CMIP5 projections, (d)–(f) white noise, (g)–(i) AR(1) realizations, and (j)–(l) power-law realizations.

our simple Monte Carlo models are adequate, the view of risk presented here is quite conservative.

4. Discussion and conclusions

In the current generation of global climate models, the risk of a decade-scale drought occurring this century is at least 50% for most of the greater southwestern United States and may indeed be closer to 80% (Figs. 9 and 10). The probability of multidecadal megadrought is also high: the likelihood of a 35-yr event is between 10% and 50% depending on how much climate change is realized during the coming century. The probability of even longer events (>50-yr, or "permanent," megadrought) is nonnegligible (5%–10%) for the most intense warming scenario (Fig. 14). Risk levels correspond to the intensity of forcing and the underlying distribution of hydroclimatic variance across the frequency continuum. The RCP8.5 scenario, for instance, depicts the highest levels of risk regardless of the underlying noise type. Likewise, the power-law noises produce higher megadrought likelihoods for each RCP than the other noises.

An obvious limitation of our work is that it is "blind" to certain aspects of dynamically driven changes in prolonged drought risk. For instance, changes in the magnitude, frequency, or teleconnection patterns of El Niño and La Niña (e.g., Coats et al. 2013a) may alter the statistics of interannual variability in ways that are not captured by our simple models. Further, megadrought statistics over the last millennium may be forcing dependent, as suggested by Cook et al. (2004), for instance, which shows that megadroughts were more common during the medieval climate era of 850–1200 CE. Another very serious limitation is imposed by the reliability of the models themselves to make realistic predictions of changes in climatological precipitation for the end of the twenty-first century.

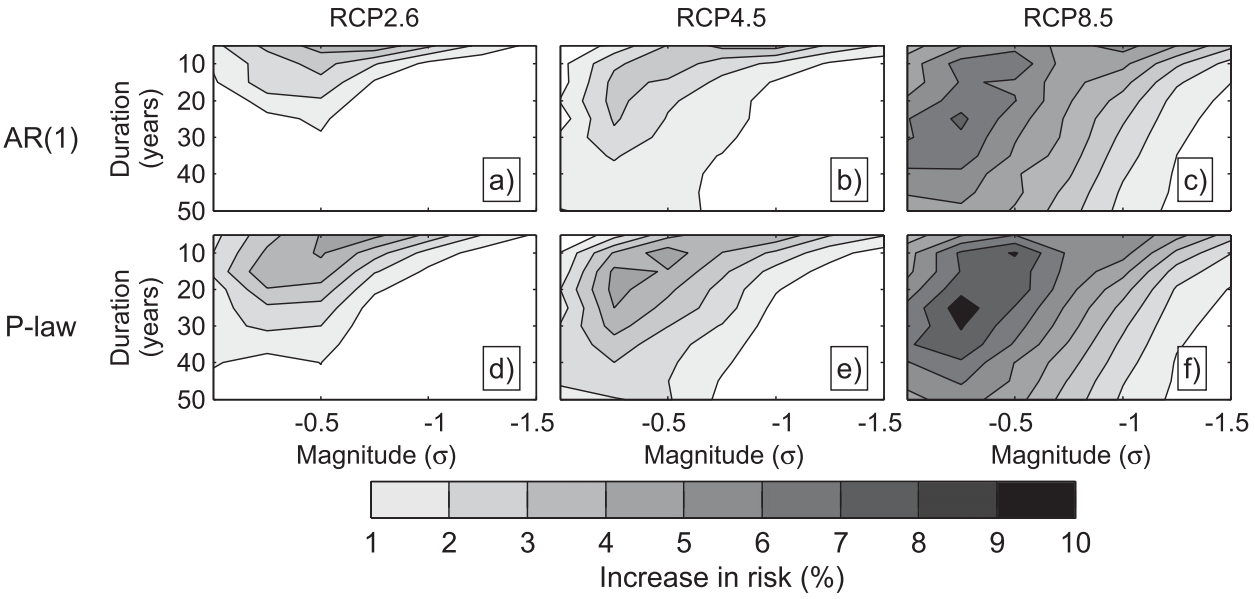

FIG. 15. Differences in duration vs magnitude risk estimates between raw CMIP5 and the two types of noises with low-frequency variability. These results are for the southwestern U.S. region, and they illustrate the difference in drought risk at a given magnitude and duration if low-frequency noise is prominent. Under the strongest forcing, the low-frequency noise models increase the risk of a multidecadal megadrought by about 8%–10%.

The projected increases in risk for the U.S. Southwest reflect forced changes in the global hydrological cycle (e.g., Held and Soden 2006; Solomon et al. 2007; Vecchi and Soden 2007; Seager et al. 2010). As such, the global picture of persistent drought risk in the CMIP5 archive (Fig. 16) bears a striking resemblance to the projected decreases in precipitation throughout many semiarid regions of the world (Diffenbaugh and Giorgi 2012; Knutti and Sedlacek 2013). It follows that prolonged drought risk is a function not only of forced changes in the global hydrological cycle and the severity of future warming, but also of the accuracy with which GCMs project large-scale changes in hydroclimate (e.g., Held and Soden 2006; Seager et al. 2007; Vecchi and Soden 2007; Seager et al. 2010). Moreover, we have based our analysis on precipitation projections, yet this variable has been notoriously challenging for GCMs to simulate accurately and large biases may remain in some models (e.g., Knutti and Sedlacek 2013; Jiang et al. 2012). Our estimates of risk are consequently only as accurate as climate model projections of changes in precipitation. An alternative approach, employed for instance by Seager et al. (2007, 2010), examines the role of large-scale dynamic and thermodynamic controls on precipitation minus evapotranspiration ($P - E$). Such studies have found that drought conditions like the Dust Bowl will become normal in the Southwest and in other subtropical dry zones. If such transitions are indeed "imminent," as stated in those studies, then the risk of decadal drought is 100%, and the risk of longer-lived events is probably also extremely high. By orienting our analysis around precipitation, the risks of prolonged drought we show here are in fact the lowest levels consistent with model simulations of future climates.

From Fig. 16 it is also clear that several other areas may be facing similar (or worse) levels of prolonged risk in the coming century. Synthesis of paleoclimatic, instrumental, and model data for these regions may lead to improvements in projecting risks in these areas and preparing appropriate adaptation and mitigation strategies. For example, high-resolution tree-ring and cave records are available from Southeast Asia (e.g., Cook et al. 2010a; Buckley et al. 2010; Sinha et al. 2007, 2011; Zhang et al. 2008) and could be used in conducting such an analysis for that region.

Despite the simplicity of our Monte Carlo model of hydroclimate in WNA, our results illustrate a crucial point for water resource managers in the region: CMIP5 models alone underestimate megadrought risk. This argument was implied in several recent studies (Cook et al. 2010b; Ault et al. 2012, 2013), but its details and implications are laid out more explicitly here (Fig. 15 specifically). Future work could refine estimates of future risks by adding additional layers of complexity to the framework we have outlined. For example, we have only used annual precipitation, which we found to be approximately normally distributed in most of WNA in most models. A more sophisticated approach could simulate the joint PDF of

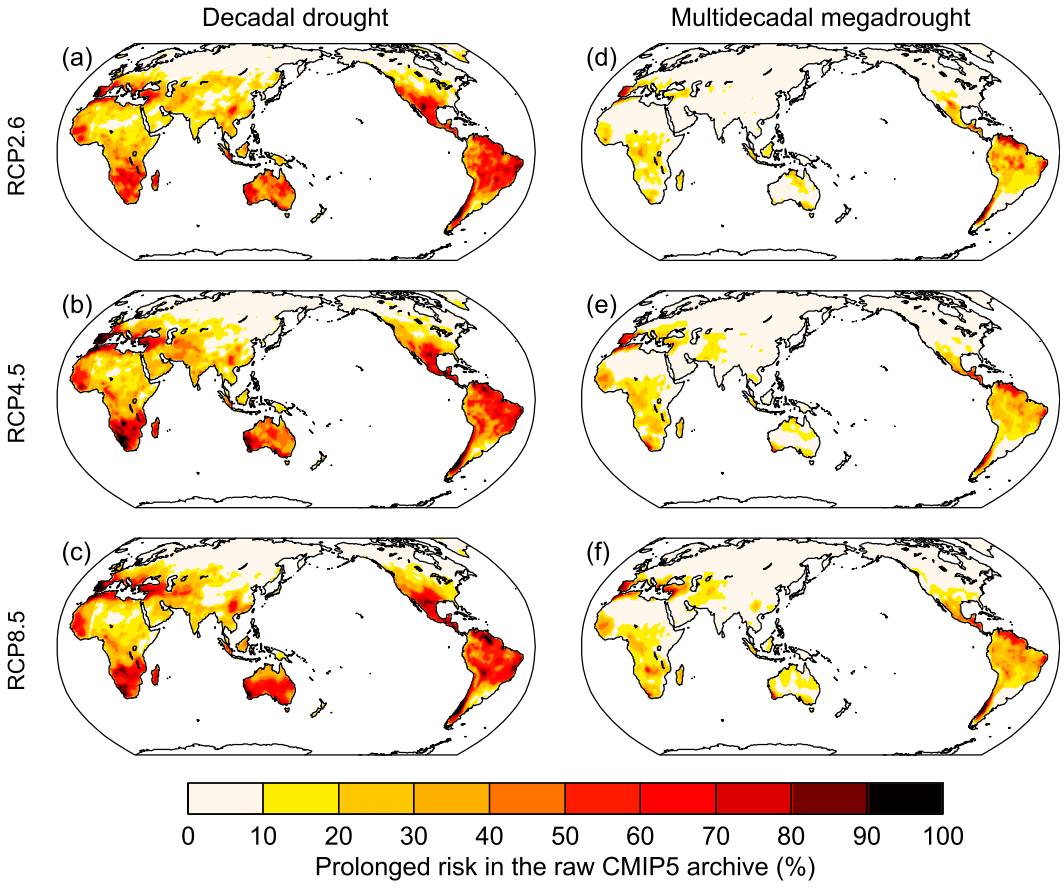

FIG. 16. Global estimates of (left) decadal and (right) multidecadal megadrought in the raw CMIP5 archive. As in Fig. 9, risk is calculated as the percent of the total number of models (27) that simulate a decadal or multidecadal megadrought. Forcing scenarios are indicated to the left of each map.

temperature and precipitation at monthly resolution, and use a more fine-tuned type of distribution and various drought indices to do so. Moreover, our noise simulations are one-dimensional in the sense that we did not build spatial autocorrelation into the noises. Developing and applying a model with realistic spatial covariance structures could help in addressing risks associated with persistent drought across large geographic scales. Likewise, it is possible that improvements in climate models, along with increasing computer power to run larger and larger ensembles, will allow for dynamically constrained assessments of megadrought risk using future generations of fully coupled climate models. In the meantime, our results provide quantitative benchmarks for water management and climate modeling communities.

5. Implications

Droughts in the past have had particularly notable human and financial costs. In the United States alone, for instance, the Federal Crop Insurance Corporation spent an average of $1.7 billion annually to compensate losses from 1980 to 2005, and this number has been increasing (Stephenson 2007). In the future, such losses might be curtailed if the full range of natural and forced hydroclimatic variability can be included in megadrought risk mitigation strategies. Here, we have described a method for combining insights from observational data and projections from climate models to estimate the risk of persistent intervals of aridity in the coming century in the U.S. Southwest. In this region where high-quality proxy records of hydroclimate have been used to constrain the underlying features of hydroclimate on decadal and longer time scales, the risk of decadal drought is at least 70% and may be higher than 90%. The risk of a multidecadal megadrought may be as high as 20%–50%, and the likelihood of an unprecedented 50-yr drought is nonnegligible (5%–10%). A number of other regions face similarly high levels of risk including southern Africa, Australia, and the Amazon basin. Moreover, future drought severity will be exacerbated by increases in temperature, implying that

our results should be viewed as conservative provided that the models depict accurate forced trends in regional hydroclimate. These findings emphasize the need to develop drought mitigation strategies that can cope with decadal and multidecadal droughts in changing climates with substantial sources of low-frequency variability.

Acknowledgments. We thank Steve Gray, Jeff Lukas, Connie Woodhouse, and the U.S. Bureau of Reclamation for assistance, and we appreciate the helpful reviews we received from Joellen Russell and Scott St. George. We are also grateful for the extensive insight and feedback we received from an anonymous reviewer. This project was supported in part by NSF graduate and NCAR-ASP postdoctoral fellowships to T. Ault, NOAA CCDD (NA07OAR4310054), NSF P2C2 (0903093) support for J. Cole, and NOAA Climate Program Office support for CLIMAS (J. Overpeck), as well as NSF EaSM2 Grant (1243125) to Cole and Overpeck. Any use of trade, product, or firm names is for descriptive purposes only and does not imply endorsement by the U.S. Government.

REFERENCES

Alley, W. M., 1984: The Palmer drought severity index—Limitations and assumptions. *J. Climate Appl. Meteor.,* **23,** 1100–1109, doi:10.1175/1520-0450(1984)023<1100:TPDSIL>2.0.CO;2.

Ault, T. R., and S. St. George, 2010: The magnitude of decadal and multidecadal variability in North American precipitation. *J. Climate,* **23,** 842–850, doi:10.1175/2009JCLI3013.1.

——, J. E. Cole, and S. St. George, 2012: The amplitude of decadal to multidecadal variability in precipitation simulated by state-of-the-art climate models. *Geophys. Res. Lett.,* **39,** L21705, doi:10.1029/2012GL053424.

——, ——, J. T. Overpeck, G. T. Pederson, S. St. George, B. Otto-Bliesner, C. A. Woodhouse, and C. Deser, 2013: The continuum of hydroclimate variability in western North America during the last millennium. *J. Climate,* **26,** 5863–5878, doi:10.1175/JCLI-D-11-00732.1.

Buckley, B. M., and Coauthors, 2010: Climate as a contributing factor in the demise of Angkor, Cambodia. *Proc. Natl. Acad. Sci. USA,* **107,** 6748–6752, doi:10.1073/pnas.0910827107.

Cayan, D. R., M. D. Dettinger, H. F. Diaz, and N. E. Graham, 1998: Decadal variability of precipitation over western North America. *J. Climate,* **11,** 3148–3166, doi:10.1175/1520-0442(1998)011<3148:DVOPOW>2.0.CO;2.

Charney, J., 1975: Dynamics of deserts and drought in Sahel. *Quart. J. Roy. Meteor. Soc.,* **101,** 193–202, doi:10.1002/qj.49710142802.

Coats, S., J. E. Smerdon, B. I. Cook, and R. Seager, 2013a: Stationarity of the tropical pacific teleconnection to North America in CMIP5/PMIP3 model simulations. *Geophys. Res. Lett.,* **40,** 4927–4932, doi:10.1002/grl.50938.

——, ——, R. Seager, B. I. Cook, and J. F. González-Rouco, 2013b: Megadroughts in southwestern North America in ECHO-G millennial simulations and their comparison to proxy drought reconstructions. *J. Climate,* **26,** 7635–7649, doi:10.1175/JCLI-D-12-00603.1.

Cook, E. R., C. A. Woodhouse, C. M. Eakin, D. M. Meko, and D. W. Stahle, 2004: Long-term aridity changes in the western United States. *Science,* **306,** 1015–1018, doi:10.1126/science.1102586.

——, R. Seager, M. A. Cane, and D. W. Stahle, 2007: North American drought: Reconstructions, causes, and consequences. *Earth Sci. Rev.,* **81,** 93–134, doi:10.1016/j.earscirev.2006.12.002.

——, K. J. Anchukaitis, B. M. Buckley, R. D. D'Arrigo, G. C. Jacoby, and W. E. Wright, 2010a: Asian monsoon failure and megadrought during the last millennium. *Science,* **328,** 486–489, doi:10.1126/science.1185188.

——, R. Seager, R. R. Heim, R. S. Vose, C. Herweijer, and C. Woodhouse, 2010b: Megadroughts in North America: Placing IPCC projections of hydroclimatic change in a long-term palaeoclimate context. *J. Quat. Sci.,* **25,** 48–61, doi:10.1002/jqs.1303.

deMenocal, P., 2001: Cultural responses to climate change during the Late Holocene. *Science,* **292,** 667–673, doi:10.1126/science.1059827.

Deser, C., A. Phillips, V. Bourdette, and H. Teng, 2012: Uncertainty in climate change projections: The role of internal variability. *Climate Dyn.,* **38,** 527–546, doi:10.1007/s00382-010-0977-x.

Diffenbaugh, N., and F. Giorgi, 2012: Climate change hotspots in the CMIP5 global climate model ensemble. *Climatic Change,* **114,** 813–822, doi:10.1007/s10584-012-0570-x.

Folland, C. K., T. N. Palmer, and D. E. Parker, 1986: Sahel rainfall and worldwide sea temperatures, 1901–85. *Nature,* **320,** 602–607, doi:10.1038/320602a0.

Fye, F. K., D. W. Stahle, and E. R. Cook, 2003: Paleoclimatic analogs to twentieth-century moisture regimes across the United States. *Bull. Amer. Meteor. Soc.,* **84,** 901–909, doi:10.1175/BAMS-84-7-901.

Haug, G. H., D. Gunther, L. C. Peterson, D. M. Sigman, K. A. Hughen, and B. Aeschlimann, 2003: Climate and the collapse of Maya civilization. *Science,* **299,** 1731–1735, doi:10.1126/science.1080444.

Hawkins, E., and R. Sutton, 2009: The potential to narrow uncertainty in regional climate predictions. *Bull. Amer. Meteor. Soc.,* **90,** 1095–1107, doi:10.1175/2009BAMS2607.1.

Held, I. M., and B. J. Soden, 2006: Robust responses of the hydrological cycle to global warming. *J. Climate,* **19,** 5686–5699, doi:10.1175/JCLI3990.1.

Hoerling, M., J. Hurrell, J. Eischeid, and A. Phillips, 2006: Detection and attribution of twentieth-century northern and southern African rainfall change. *J. Climate,* **19,** 3989–4008, doi:10.1175/JCLI3842.1.

Hunt, B. G., 2011: Global characteristics of pluvial and dry multiyear episodes, with emphasis on megadroughts. *Int. J. Climatol.,* **31,** 1425–1439, doi:10.1002/joc.2166.

Jiang, J. H., and Coauthors, 2012: Evaluation of cloud and water vapor simulations in CMIP5 climate models using NASA "A-Train" satellite observations. *J. Geophys. Res.,* **117,** D14105, doi:10.1029/2011JD017237.

Kantelhardt, J., E. Koscielny-Bunde, D. Rybski, P. Braun, A. Bunde, and S. Havlin, 2006: Long-term persistence and multifractality of precipitation and river runoff records. *J. Geophys. Res.,* **111,** D01106, doi:10.1029/2005JD005881.

Knutti, R., and J. Sedlacek, 2013: Robustness and uncertainties in the new CMIP5 climate model projections. *Nat. Climate Change,* **3,** 369–373, doi:10.1038/nclimate1716.

Koscielny-Bunde, E., J. W. Kantelhardt, P. Braun, A. Bunde, and S. Havlin, 2006: Long-term persistence and multifractality of

river runoff records: Detrended fluctuation studies. *J. Hydrol.,* **322,** 120–137, doi:10.1016/j.jhydrol.2005.03.004.

Leblanc, M., S. Tweed, A. Van Dijk, and B. Timbal, 2012: A review of historic and future hydrological changes in the Murray-Darling Basin. *Global Planet. Change,* **80–81,** 226–246, doi:10.1016/j.gloplacha.2011.10.012.

Meko, D. M., C. A. Woodhouse, C. A. Baisan, T. Knight, J. J. Lukas, M. K. Hughes, and M. W. Salzer, 2007: Medieval drought in the upper Colorado River Basin. *Geophys. Res. Lett.,* **34,** L10705, doi:10.1029/2007GL029988.

——, ——, and K. Morino, 2012: Dendrochronology and links to streamflow. *J. Hydrol.,* **412,** 200–209, doi:10.1016/j.jhydrol.2010.11.041.

Milotti, E., 1995: Linear processes that produce 1/*f* or flicker noise. *Phys. Rev. E,* **51,** 3087–3103, doi:10.1103/PhysRevE.51.3087.

Mitchell, T. D., and P. D. Jones, 2005: An improved method of constructing a database of monthly climate observations and associated high-resolution grids. *Int. J. Climatol.,* **25,** 693–712, doi:10.1002/joc.1181.

Moss, R. H., and Coauthors, 2010: The next generation of scenarios for climate change research and assessment. *Nature,* **463,** 747–756, doi:10.1038/nature08823.

Pelletier, J. D., 2008: *Quantitative Modeling of Earth System Processes.* 1st ed. Cambridge University Press, 294 pp.

——, and D. Turcotte, 1997: Long-range persistence in climatological and hydrological time series: Analysis, modeling and application to drought hazard assessment. *J. Hydrol.,* **203,** 198–208, doi:10.1016/S0022-1694(97)00102-9.

Penland, C., and P. D. Sardeshmukh, 2012: Alternative interpretations of power-law distributions found in nature. *Chaos,* **22,** 023119, doi:10.1063/1.4706504.

Routson, C. C., C. A. Woodhouse, and J. T. Overpeck, 2011: Second century megadrought in the Rio Grande headwaters, Colorado: How unusual was medieval drought? *Geophys. Res. Lett.,* **38,** L22703, doi:10.1029/2011GL050015.

Seager, R., and Coauthors, 2007: Model projections of an imminent transition to a more arid climate in southwestern North America. *Science,* **316,** 1181–1184, doi:10.1126/science.1139601.

——, N. Naik, and G. A. Vecchi, 2010: Thermodynamic and dynamic mechanisms for large-scale changes in the hydrological cycle in response to global warming. *J. Climate,* **23,** 4651–4668, doi:10.1175/2010JCLI3655.1.

Shanahan, T. M., and Coauthors, 2009: Atlantic forcing of persistent drought in West Africa. *Science,* **324,** 377–380, doi:10.1126/science.1166352.

Sinha, A., K. G. Cannariato, L. D. Stott, H. Cheng, R. L. Edwards, M. G. Yadava, R. Ramesh, and I. B. Singh, 2007: A 900-year (600 to 1500 A.D.) record of the Indian summer monsoon precipitation from the core monsoon zone of India. *Geophys. Res. Lett.,* **34,** L16707, doi:10.1029/2007GL030431.

——, L. Stott, M. Berkelhammer, H. Cheng, R. L. Edwards, B. Buckley, M. Aldenderfer, and M. Mudelsee, 2011: A global context for megadroughts in monsoon Asia during the past millennium. *Quat. Sci. Rev.,* **30,** 47–62, doi:10.1016/j.quascirev.2010.10.005.

Solomon, S., D. Qin, M. Manning, Z. Chen, M. Marquis, K. Averyt, M. Tignor, and H. L. Miller, Eds., 2007: *Climate Change 2007: The Physical Science Basis.* Cambridge University Press, 996 pp.

Stahle, D. W., F. K. Fye, E. R. Cook, and R. D. Griffin, 2007: Tree-ring reconstructed megadroughts over North America since AD 1300. *Climatic Change,* **83,** 133–149, doi:10.1007/s10584-006-9171-x.

——, and Coauthors, 2011: Major Mesoamerican droughts of the past millennium. *Geophys. Res. Lett.,* **38,** L05703, doi:10.1029/2010GL046472.

Stephenson, J. B., 2007: Climate change: Financial risks to federal and private insurers in coming decades are potentially significant. Committee on Homeland Security and Governmental Affairs, U.S. Govt. Accountability Office, 22 pp. [Available online at http://www.gao.gov/products/GAO-07-760T.]

Vasseur, D., and P. Yodzis, 2004: The color of environmental noise. *Ecology,* **85,** 1146–1152, doi:10.1890/02-3122.

Vecchi, G. A., and B. J. Soden, 2007: Global warming and the weakening of the tropical circulation. *J. Climate,* **20,** 4316–4340, doi:10.1175/JCLI4258.1.

Wells, N., S. Goddard, and M. J. Hayes, 2004: A self-calibrating Palmer drought severity index. *J. Climate,* **17,** 2335–2351, doi:10.1175/1520-0442(2004)017<2335:ASPDSI>2.0.CO;2.

Woodhouse, C. A., and J. T. Overpeck, 1998: 2000 years of drought variability in the central United States. *Bull. Amer. Meteor. Soc.,* **79,** 2693–2714, doi:10.1175/1520-0477(1998)079<2693:YODVIT>2.0.CO;2.

Zhang, P., and Coauthors, 2008: A test of climate, sun, and culture relationships from an 1810-year Chinese cave record. *Science,* **322,** 940–942, doi:10.1126/science.1163965.